Ophthalmology Research (in press, 1-2018) pw:42o1bs
Original research article

Efficacy S-formula and kinetics of non-oxygen-mediated (type-I) and oxygen-mediated (type-II) corneal cross-linking

Jui-Teng Lin*
New Vision Inc. Taipei, Taiwan 103
* jtlin55@gmail.com

ABSTRACT

Aims: To derive analytic formulas for the overall efficacy of corneal collagen crosslinking (CXL) based on coupled kinetic equations including both non-oxygen-mediated (NOM) and oxygen-mediated (OM) type-II mechanisms.

Study design: modeling the kinetics of CXL

Place and Duration of Study: Taipei, Taiwan, between June, 2017 and January. 2018.

Methodology: Coupled kinetic equations are derived under the quasi-steady state condition for the 3-pathway mechanisms of CXL. For type-I CXL, the riboflavin triplet state [T_3] may interact directly with the stroma collagen substrate [A] under NOM, or with the ground-state oxygen [O_2] to form reactive oxygen species [O-] under OM. For type-II process, [T_3] interacts with [O_2] to form a singlet oxygen [$^1O_2$]. Both reactive oxygen species (ROS), [O-] and [$^1O_2$], can relax to [O_2], or interact with the extracellular matrix (or the stroma substrate [A]) for crosslinking.

Results: In the first 5 to 20 seconds, CXL efficacy is governed by both type-I and –II mechanisms, and after that period type-I, NOM is the predominant contribution, while oxygen for OM only plays a limited and transient role, in contrary to the conventionally believed OM-dominant mechanism. The riboflavin profile has a much slower depletion rate than that of oxygen profile. The ratio between NOM-type-I and OM depends on the relative initial concentration of [A] and [$^1O_2$] and their diffusion depths in the stroma. The overall CXL efficacy is proportional to the UV light dose (or fluence), the riboflavin, C (z, t), and oxygen, [O_2], initial concentration, where efficacy is limited by the depletion of either C (z, t) or [O_2].

Conclusion: Resupply of riboflavin and/or oxygen concentration under a controlled-concentration-method (CCM) during the UV exposure may improve the overall efficacy, specially for the accelerated CXL which has lower efficacy than the standard Dresden low-power (under non-controlled concentration).

Keywords: Corneal crosslinking; corneal keratoconus; efficacy; kinetic modeling; oxygen; riboflavin; ultraviolet light; photodynamic therapy.

1. INTRODUCTION

Photochemical kinetics of corneal collagen crosslinking (CXL) and the biomechanical properties of corneal tissue after CXL have been reported and summarized in a recent book [1]. The safety and efficacy issues of CXL have been reported theoretically [2-14]. The critical parameters influencing the efficacy of CXL include: initial concentration and diffusion depth of riboflavin (RF) (for type-I CXL) and oxygen (for type-II CXL), quantum yield, UV light intensity, dose and irradiation duration. Most of the previous models [2-6] are not accurate due to the oversimplified assumptions of constant RF profiles, or non-depleted RF, or UV light intensity following the simple Beer-Lambert law (BLL).

Standard (Dresden) protocols were revised for faster (accelerated) CXL based on Bunsen-Roscoe law (BRL) having a limited validation of UV maximum intensity [13]. Controversial efficacy issues of Dresden versus accelerated corneal crosslinking (A-CXL) have been discussed recently by Lin [13] and a concentration-controlled method (CCM) to improve the efficacy of A-CXL was also proposed [14].

Schumacher et al [3] reported the NOM-type-I CXL, in contrast to Kling et al [5] claiming that oxygen-mediated type-II played the critical role of CXL efficacy. Furthermore, Kamaev et al [2] claimed that CXL is NOM-type-I dominant, while the OM-type-II only plays a limited and transient role. If Kling et al were correct, then all the reported results of epi-on CXL would not be possible, since only minimum oxygen supply is available [1].

The photochemical kinetics of type-II process and the role of oxygen was reported previously [10]. This article intends to resolve the non-conclusive issues about the role of oxygen in CXL efficacy which should be governed by both OM and NOM, 3-pathway processes, rather than the conventionally believed type-II only (oxygen-mediated) mechanism [5]. Efficacy formulas will be presented to demonstrate the factors determining the relative contribution of NOM and OM.

The coupling between OM and NOM and their efficacy will be analyzed by the derived S formulas, which, to my knowledge, are for the first time available in CXL, although similar kinetics were presented for anti-cancer photodynamic process [15,16], which, however, have ignored the NOM type-I mechanism. This study will focus on the analytic formulas and the important features resulted from these S formulas, whereas detailed numerical simulations will be presented elsewhere.

2. MATERIAL AND METHODS

2.1 Photochemical kinetic (Type-I and –II)

The photochemical kinetics of CXL is shown in Fig. 1 for both type-I and –II. Greater detailed kinetic of type-II only was published in my prior work [10]. This study will present the combined kinetics. Fig. 1 shows the depletion profile of oxygen which defines the contribution of type-I and type-II in different stage. Typical depletion time of oxygen is about 5 to 15 seconds, for light intensity of 30 to 3 mW/cm^2, per measured data of Kamaev et al [2], and takes about 10 minutes for the oxygen to be resupplied or replenished to about 1/3 of its initial state.

Both type-I and type-II reactions can occur simultaneously, and the ratio between these processes depends on the type of photosensitizers (PS) used, the concentrations of PS, substrate and oxygen, the kinetic rates involved in the process, and the light intensity, dose, PS depletion rate etc. More details will be shown later.

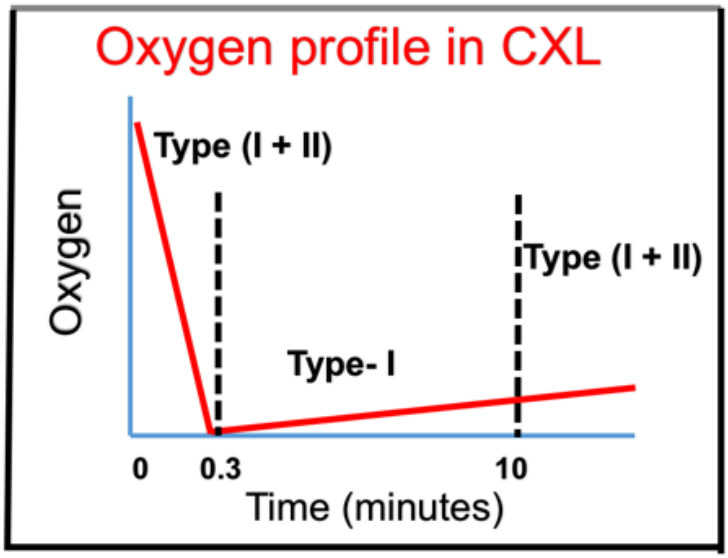

Fig. 1 Schematics of the oxygen profiles during the CXL process; in the transient stage, both type-I and –II coexist until the oxygen is depleted; then type-I dominates before the oxygen is resupplied or replenished [10].

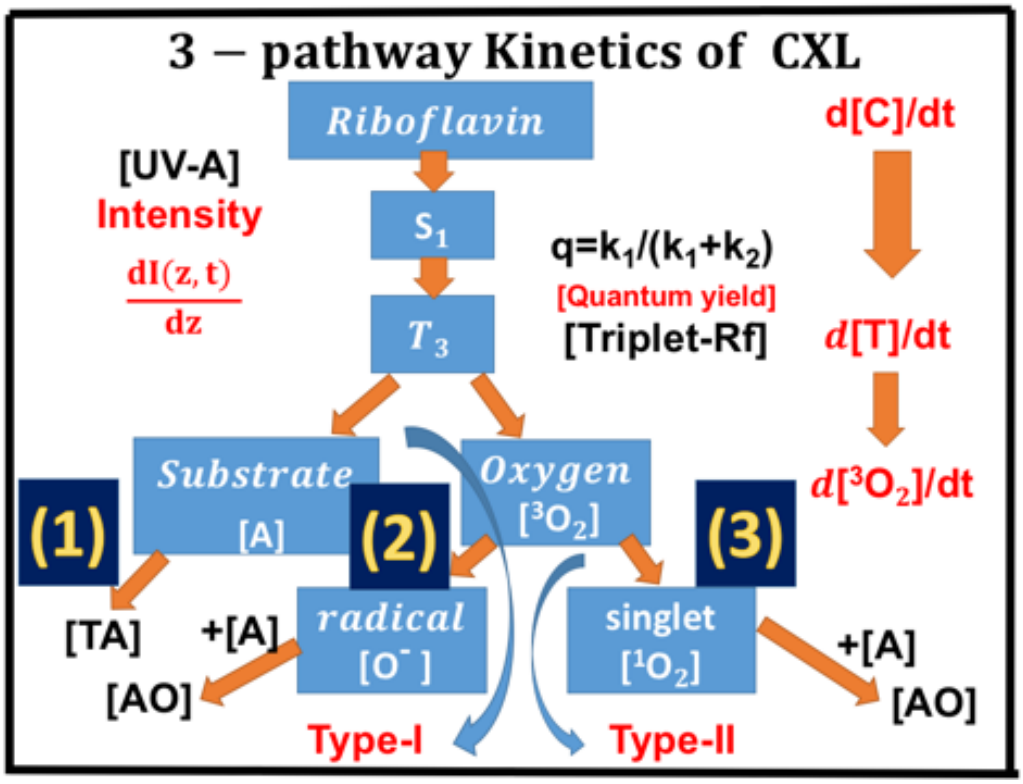

Fig. 2. The kinetics of CXL, where $[S_0]$, $[S_1]$ and $[T_3]$ are the ground state, singlet excited state, and triplet excited state of RF molecules. Three pathways are shown for both type-I and type-II process. Ground state oxygen may couple to T_3 to form either singlet oxygen [O*], or other reactive radicals [O-]. In type-I pathway, T_3 can interact directly with the collagen substrate (A); or with the oxygen (O_2) to generate a superoxide anion (O^-); in type-II pathway, T_3 interacts with the ground oxygen (O_2) to form a singlet oxygen (O*) [13].

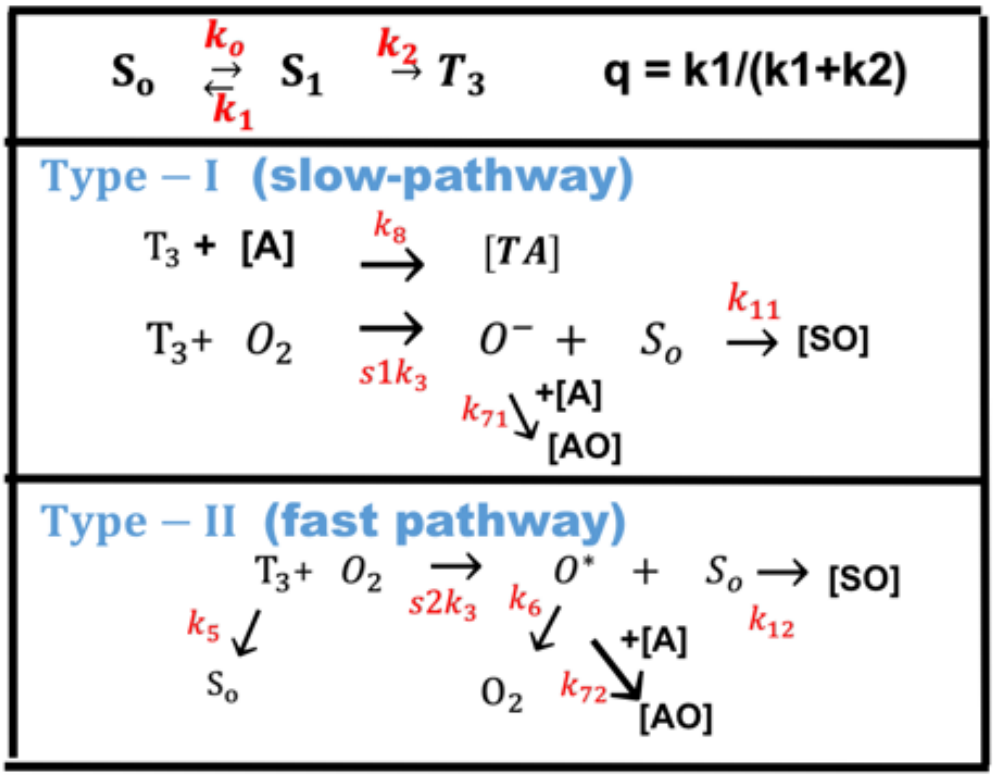

Fig. 3. The kinetics of CXL showing the rate constants associate with Fig. 2 [10,17].

As shown in Fig. 2 and 3, the CXL process is described as follows. The ground state RF molecules are excited by the UV light to its singlet excited state (S_1), which could be relaxed to its ground state or to a triplet excited state (T_3). In type-I process, (T_3) could interact directly with the stroma collagen substrate [A] for crosslinking, or could interact with the ground state oxygen, [O_2], to form reactive superoxide anion radicals [O-]. For type-II process, (T_3) interacts with [O_2] to form oxygen singlet [$^1O_2$]. The reactive oxygen radicals (ROS), [$^1O_2$] or [O-], could be relaxed to its ground state oxygen [O_2], or interacts with the stroma substrate [A] to treat corneal ulcers or to form cross linking.

The kinetics shown in Fig.2 includes both oxygen-mediated (OM) related to the reactive oxygen radicals (ROS), [$^1O_2$] or [O-]; and non-oxygen-mediated (NOM) term in type-I given by the direct interaction of the triplet (T_3) with the stroma collagen substrate [A].

The kinetic equations (based on the kinetics of Fig. 3) for the concentration of various components are shown by using short-hand notations: C (z, t) and C*(z, t) for the RF ground and singlet state [S_0] and [S_1]; X (z, t) and X*(z, t) for the ground state [$^3O_2$] and singlet oxygen [O*], Y*(z, t) for superoxide anion radicals [O-], T (z, t) for the

RF triplet state (T_3), and [A] for the available extracellular matrix substrate; given by [10,17]

$$\frac{\partial C(z,t)}{\partial t} = -k_0 C + k_1 C^* + K_4 T - K_5 (C + s) \quad (1.a)$$

$$\frac{\partial C^*(z,t)}{\partial t} = k_0 C - k_1 C^* - k_2 C^* \quad (1.b)$$

$$\frac{\partial T(z,t)}{\partial t} = k_2 C^* - K_3 T \quad (1.c)$$

$$\frac{\partial X^*(z,t)}{\partial t} = s_2 k_3 X T - K_2 X^* \quad (1.d)$$

$$\frac{\partial Y^*(z,t)}{\partial t} = s_1 k_3 X T - K_1 X^* \quad (1.e)$$

$$\frac{\partial X(z,t)}{\partial t} = k_6 X^* - (s_1 + s_2) k_3 X T + P \quad (1.f)$$

$$\frac{\partial [A]}{\partial t} = -(k_{72} X^* + k_{71} Y^* + k_8 [T])[A] \quad (1.g)$$

where, $K_4 = (k_5 + k_3 X)$; $K_5 = [k_{12} X^* + k_{11} Y^*]$, which includes both OM terms for type-II ($k_{12} X^*$) and type-I ($k_{11} Y^*$); $K_3 = (k_3 X + k_5 + k_8 [A])$; and $K_2 = k_6 + k_{12}(C+s) + k_{72}[A]$; $K_1 = k_{11}(C+s) + k_{71}[A]$; and s is a low concentration correction related to the diffusion of singlet oxygen [17]. Where $k_{12} C$ can be neglected, when $k_{12} C << k_6$ or $k_{72}[A]$, to avoid the C dependence of K_1 or K_2, when deriving the analytic formulas.

In Eq. (1.f), s_2 and s_1 are the fraction of triplet-state and oxygen reactions to produce $^1O_2$ (in type-II) and other ROS (in Type I) reactions. Eq. (1.f) includes an oxygen source term given by $P=(1-X/X_0)\, P_0$, with a maximum rate constant P_0, where $(1-X/X_0)$ is included to avoid the negative value of oxygen. We note, in Eq. (1.a), that $-k_0 C$ and $-K_5 C$ are related to the RF depletion, whereas $+k_1 C^*$ and $K_4 T$ are the regeneration of RF (due to the reaction of [T] and oxygen). Therefore, the presence of oxygen will reduce the RF depletion due to the NOM-type-I mechanism. However, the conventionally belief, that there is no RF depletion in type-II pathway is not correct, because RF is depleted to produce triplet state given by its quantum yield, $q = k_2/(k_1 + k_2)$, in both type-I and type-II. More details will be shown later.

Compared to our previous type-II only model [10], we have added new terms in Eq. (1.a): the type-I NOM term, $k_8[A]$, and the OM term, $k_{11} Y^*$, due to other radicals, [O-]. Eq. (1.f) also includes extra NOM and OM terms, $k_{72}[A] + k_{71} Y^*$.

The dynamic UV light intensity is given by

$$\frac{\partial I(z,t)}{\partial z} = -A'(z,t)I(z,t) \qquad (2.a)$$

$$A'(z,t) = 2.3[(a' - b')C + b'C_0F' + Q] \qquad (2.b)$$

where F'(z)=1-0.25z/D, with D being the initial diffusion depth of RF; and a=83.6 λ, λ being the UV light wavelength; a' =204 (1/%/cm) and b' are the extinction coefficients of RF and the photolysis product, respectively; Q=13.9 (1/cm) is the absorption coefficient of the stroma at the UV wavelength.

We note that Eq. (1) was also presented by Kim et al [16], however, they have assumed a constant UV intensity, i.e., Eq. (2) are not proposed. They also ignored the contribution from the type-I term, k_8[A], since type-II is dominant in their anti-cancer process. Most of the previous model have also ignored the dynamic of UV intensity given by Eq. (2) and the depth-dependent profile of RF and UV intensity [2-6]. Accurate solutions of Eq. (1) and (2) require numerical simulations. For analytic ofrmulas, I will use an effective A(z,t) or its mean value, such that A'(z,t) becomes time-independent in solving Eq. (1).

Eq. (1.f) includes both OM and NOM. Eq. (1.c) includes one extra term, k_8[A], for the reduction of the triplet RF due to its direct coupling to the collagen substrate [A], when type-I process occurs simultaneously with type-II. This extra RF depletion term was ignored in previous modeling [2-6]. In Eq. (5.d) for the oxygen concentration, we have included a source term (P) to count for the situation when there is an external continuing supply, or nature replenishment, besides the initial oxygen in the stroma, which will be defined by an oxygen diffusion function later. In general, P is time-dependent and can be positive or negative [15].

The kinetic equations (1) and (2) may be numerically calculated to find the CXL efficacy, which however is too complex for us to analyze the roles of each of the parameters. For comprehensive modeling we will use the so-called quasi-steady state assumption [15] described as follows. The life time of the singlet and triplet states of photosensitizer (C* and T) and the singlet oxygen (X*) are very short (ns to μs time scale) since they either decay or react with cellular matrix immediately after they are created. Thus, one may set the time dependences, dC*/dt=dT/dt=dX*/dt=0, or the quasi-steady-state state. We first find the steady-state solutions: T= aqIG/k_3, X*= s_2(aqIG)/K_2; Y*= s_1(aqIG)/K_1, which in turn gives

$$\frac{\partial C(z,t)}{\partial t} = -(aqI)[g + K_{12}\, G] \qquad (3.a)$$

$$\frac{\partial [O_2]}{\partial t} = -(N aqI)[s_1 + s_2]G + P \qquad (3.b)$$

$$G(z,t) = C[O_2]/([O_2] + k) \qquad (3.c)$$
$$g(z,t) = (k_8/k_3)[A]/([O_2] + k) \qquad (3.d)$$

where q is the triplet state [T] quantum yield given by q=$k_2/(k_1+k_2)$; K_{12}= $(s_1k_{11}/K_1+ s_2k_{12}/K_2)$; $K_1= k_{11}(C+s)+k_{71}[A]$; $K_2= k_6+ k_{12}(C+s)+k_{72}[A]$; $k= k_5/k_3+ (k_8/k_3)[A]$.
In Eq. (3.b), we added a new parameter (N) to fit the measured data of oxygen time-profile (to be discussed later).
The above coupled equations will be solved under an initial conditions having initial profiles defined by their diffusion depths, D (for RF), D'/ (for oxygen), and 2D (for UV intensity, given by $C_0(z)$=1-0.5z/D, $[O_0](z)$=1-0.5z/D, and $I_0(z)$=1-0.5z/ (2D), respectively.

2.2 The S formulas for overall efficacy

The normalized efficacy defined by Ceff =1-[A]/$[A]_0$ = 1-exp(-S), with S-function for type-I (S_1) and type-II (S_2) defined by Eq. (1.f) and can be further derived as follows. The type-I efficacy defined by Eq. (1.f) may be further expressed by rate equation of conversion of collagen monomers [M] to polymers, where the NOM term of Eq. (1.a), g= k_{83}[A]/($[O_2]$+k), in Eq. (3.d) and (1.f), is replaced by an overall rate constant (K) including all polymerization chain reactions. The more accurate S_1 is given by [11]

$$S_1 = \int_0^t \left(\sqrt{aqgK\,CI} + f\,k_{71}[A]Y^*\right)dt \qquad (4.a)$$

where K' is an overall rate constant (excluding the k_{71} pathway) for the NOM reactions; and the ROS-mediated term is given by the second term, k_{71}Y*[A], Y* being the singlet oxygen concentration, which was ignored in our previous CXL type-I modeling [11].
Similarly, the S-function for type-II (S_2) is given by, from Eq. (1.f),

$$S_2 = \int_0^t (f\,k_{72}[A]X^*)dt \qquad (4.b)$$

Using the steady-state value of [T], [X*] and [Y*], the associate S-functions for the efficacy for type-I and type-II are given by, from Eq. (4),

$$S_1 = \int_0^t [\sqrt{aqgK\,C(z,t)I(z,t)} + (fs_1aqK')I(z,t)G]dt \qquad (5.a)$$

$$S_2 = ((fs_2aq)\int_0^t K'I(z,t)G)\,dt \qquad (5.b)$$

where K'= 1/ (1+C+0.65 [A]), in which we have used the values [2]: k_{72}=k_{71}=1.7x10^5 (1/s), k_6=k_{11}=k_{12} =2.6x10^5 (1/s).

The first term in Eq. (5.a) relates with the direct coupling of triplet state [T] with the substrate [A] under hypoxic conditions or any other NOM reactions; and the second term relates with the (ROS)-mediated reactions (in type-I). *f* is the fraction of all ROS (including singlet oxygen) interacting with acceptors [A], or the oxygen-mediated (NOM) reactions in type-I and type-II. s_2 and s_1 are the fraction of $[O_2]$ interacting with [T] to produce singlet oxygen (in type-II) and other ROS (in type-I), respectively; with typical values of (for RF) s_1=0.01 and s_2=0.49; or singlet oxygen is the dominant ROS. In comparision, for rose bengal, s_1=0.2 and s_2=0.8 [17]. The overall CXL-efficacy is given by Ceff=0.5[CX1 + CX2], with CX1=1-exp(-S_1), CX2=1-exp(-S_2).

3. Results and Discussions

3.1 Coupling between type-I and type-II

We note that Eq. (3.a) includes the NOM term (with coupling term $[O_2]$+k) for type-I, g= $[k_8[A]/k_3]/([O_2]+k)$, and the OM, or ROS-mediated oxygen term, $K_{12}G$, which has two terms s_1k_{11}/K_1 and s_2k_{12}/K_2 contributed by type-I and –II, respectively. With the absence of oxygen (o when oxygen is depleted after the transient 5 to 20 seconds), $[Q_2]$=0, G=0, g= $[k_8[A]/k_3]/k$, and Eq. (3.a) reduces to type-I NOM-CXL, with efficacy given first term of Eq. (5.a).

In contrast, when g<<$K_{12}G$, Eq. (3.a) reduces to ROS-mediated CXL which requires oxygen, singlet oxygen or other ROS as the key elements. Other than the above special situations, type-I and type-II CXL are closely coupled by the interaction term, $K_{12}G$, in Eq. (5.a), which has both OM terms.

The ratio between OM and NOM-type-I for RF depletion, is given by R=$K_{12}G/g$ =$C(z)[O_2]K_{12}/(k_8/k_3)[A]$, with K_{12} = s_2/ (1+(C+s)+ 0.65 [A]). For typical values of [2,4] k_8/k_3=0.05, k_{72}/k_6 = k_{71}/k_6=0.65 and s_2=0.5; and initial value C_0=0.1, $[O_0]$=7.3. R=0.15/(0.05[A])=3/[A]. Therefore, R=3, when [A]=1; R=0.3, when [A]=10.

For the situation that R<<1 (or $K_{12}G$<<g, with [A]>10), the major depletion of C(z,t) is caused by the NOM term. Type-II OM dominant process claimed by Kling et al [8] is valid only for the special case that [A]<1, or R>>1, such as rose bengal CXL in green light. However in RF-CXL, type-I shodul be dominant. Typical values of above rate constants depend on the properties of the photosensitizers (PSs). For ALA and Photofrin used in anti-cancer reported by Zhu et al [6] s_1 = 0.2, s_2= 0.8; and s_1 = 0.01, s_2= 0.49 for riboflavin CXL.

The initial concentration profiles (at t=0) of the RF and oxygen may be calculated or measured based on Fick's second law of diffusion [9,10,14]. For analytic solution, we will chose the distribution profile given by [3,6]: F(z,D) = 1 – 0.5z/D for RF solution, or C(z,t=0)=C_0F(z), with a diffusion depth D in the stroma; and F'(D',z) =1 – 0.5z/D'

for the oxygen initial concentration, or $X(z,0)= X_0F'(D',z)$, with a different diffusion depth D'. The typical diffusion depths are: D is 200 to 500 um and D' is 100 to 200 um.

The prior work of Zhu and Kim et al [16,17], Schumacher et al [3], and Kling [5] assumed a constant UV light intensity and ignored the RF depletion, i.e., $X(z,t) =X_0$, which is a constant in Eq. (2.b), based on the conventional Beer-Lambert law which overestimated the A(z,t) as its initial value when t>0. The prior work also assumes a flat RF concentration, or F(z,t)=1 and used an oversimplified model to assume no absorption of the photolytic products, or b'=0. The extra RF depletion term (g) due to direct coupling of [T] and [A], in Eq. (3.a), was ignored in previous model work [2-6,16]. Therefore, our model system based on Eq. (3)and (5) is much more accurate than the prior works in describing the CXL process when type-I and type-II coexist, specially for the initial stage prior to the oxygen depletion, and after the transient state with type-I dominant.

According to the proposed mechanism of Kamaev et al [2], under aerobic conditions, they believe that CXL in the cornea is initiated due to the direct interaction between the substrate and excited RF triplets, with singlet oxygen playing a limited and transient role in the process. In contrary, Kling et al [3] believed that type-II is the predominant mechanism. Our new modeling system demonstrated theoretically that CXL using RF as the PS is predominated by the NOM term of type-I, or the direct coupling of triplet RF to the substrate [A], since the OM pathways (in both type-I and II) via singlet oxygen play a limited and transient role in the process per Kamaev et al [2], who proposed the mechanisms but did not develope the detailed macroscopic equations shown in this study.

3.2 Analytic Formulas

We will first derive the analytic formulas for the efficacy of type-I and -II CXL as follows. Typical depletion time of oxygen is about 5 to 15 seconds, for light intensity of 30 to 3 mW/cm^2, per measured data of Kamaev et al [2], and takes about 10 minutes for the oxygen to recover to 1/3 of its initial state.

For the situation that $R<<1$ (or $K_{12}G<<g$, with [A]>10), the major depletion of C(z,t) is caused by the NOM term. Solving for Eq. (3.a) to obtain an approximated $C(z,t)= C_0Fexp(-Bt)$, with $B =aqgI(z)$, with I(z) given by Eq. (2) and A' given by its mean value or steady-state fit-value such that it becomes time-independent [9,11]. Using this C(z,t) we may solve for $[Q_2]$ in Eq. (3.b). We note that the depletion time (t_0) of oxygen is about 5 to 20 seconds, which is much shorter than 1/b, to be shown later.

For the other situation that R>>1 (or $K_{12}G$>>g, with [A]<0.5), the major depletion of C(z,t) is caused by the OM term. Solving for $dC/dt=-bK_{12}C^2$, with b=*ag*I(z) to obtain $C(z,t)=C_0F/(1+K_{12}C_0Fbt)$. In general, for the range of [A]=2 to 5, R has a range 0.6 to 1.5, one must solve for both NOM and OM terms, i.e., type-I and type-II depletion of RF must be considered simultaneously with numerical simulation (to be shown elsewhere). We will consider the analytic cases as follows.

Case (1) and for g>>$K_{12}G$, without oxygen source term (or for the transient stage), P=0, analytic solution is given by the solution of the nonlinear equation of the UV light exposure time (t)

$$Y_2-Y_1=0.5N(b/B)C_0F[1-\exp(-Bt)] \quad (6.a)$$

$$t=(1/b)\ln[Y_2-Y_1-k] \quad (6.b)$$

with $Y_2=[O_2]+k\ln[O_2]$, $Y_1=[O_0]F'+k\ln([O_0]F')$; $B=b(g+K_{12})$, is the effective rate constant for RF depletion. $[O_0]$ is the oxygen initial concentration. Given Eq. (6.b), we may plot the curve for t vs. $[O_2]$, and rotated for $[O_2]$ vs. t, which also give the profile for G(z,t) vs. t, and integration of $KI(z)C(z,t)G(z,t)$, $s_1I(z)G_0(z,t)$ and $s_2I(z)G(z,t)$ give us the S_1 and S_2 function defined by Eq. (5).

Case (2). For P>0, and for g<<$K_{12}G$, I also obtained the approximated solution for oxygen

$$[O_2] = [O_0]F' - N\ln[1 + b't] + N'P_0t \quad (7)$$

where b'= $K_{12}b$, with $K_{12}=(s_1+s_2)(C_0F)/(1+0.65\ [A])$, for (C+s)<<1, and $k_{72}/k_6=0.65$; b=*aq*I(z), with *a*=0.31, I(z) in mW/cm^2; $P=(1-[O_2]/[O_0])P_0$; F'(z,D) = 1 – 0.5z/D' and F(z,D) = 1 – 0.5z/D; D' and D are the initial diffusion depth of oxygen and RF, respectively. Eq.(7) shows that $[O_2]$ is a decreasing function of z and UV intensity, since b=*aq*I(z). N and N' are fit parameters to be found numerically, withN'=(

In Eq. (6) and (7), I added a new parameter (N) to fit the measured data that oxygen is depleted at about 10 to 20 s, for an intensity of 3 mW/cm^2, (or dose of 30 to 60 mW/cm^2), per measured data of Kamaev et al [2]. The fit N is calculated from Eq. (7), for $b=0.3E_0=0.3I_0t$ (at z=0, F=F'=1), $C_0=0.1$, $K_{12}=0.5C_0$, $N=[O_0]/\ln(1+0.15\ C_0E_0)$. Therefore, N= (14,11.4, 9.2, 8.6), for dose E_0 = (45, 60,80, 90) mJ/cm^2, when $[O_2]$ is completely depleted, where E_0=60 mJ/cm^2 represents [t=20 s for I_0 = 3 mW/cm^2], or [t=7 s for I_0 = 30 mW/cm^2] etc.

Using $C(z,t)=C_0F/[1+(K_{12}C_0F)bt]$ and time integral of bG, with G approximated by C(z,t) in Eq. (5.b), I obtain the analytic formula for the S-function for the case of g<<$K_{12}G$ and P=0,

The efficacy of NOM-type-I (S1) and OM-type-II (S2) can be calculated by the time

integral of [A]sqrt[IC(z,t)] and [A]IC(z,t)[O_2] as shown by Eq.(5), respectively, given by [10,11]:

$$S_1 = \mathrm{E}'[\mathrm{A}]\sqrt{4\mathrm{K}'\,\mathrm{C}_0\mathrm{F}(\mathrm{z})\exp(\mathrm{Az})/(aq\mathrm{I}_0)} \qquad (8.a)$$

with E'(z,t) = [1-exp(-0.5bt)], for the case that g>>K_{12}G and after oxygen is depleted. K' is an effective rate constant for polymerization [11]. Eq. (8.b) shows that S is a decreasing function of I_0, but increasing function of z (for steady-state). We note that Eq. (8.a) is available only for the case that g=1, or when oxygen is depleted such that [O_2] in g-fucntion can be neglected; otherwise, numerical simulatioj is needed. For transient state, S1 has optimal depth (z*) which is proportional to ln(aE_0)/A.

Uing Eq. (7) and the approximated C(z,t), I also obtained the approximated fucntion,

$$S_2 = 0.32[\mathrm{A}](\mathrm{H}\ln(1+\mathrm{b}'\mathrm{t}) + \mathrm{H}'P_0t^2) \qquad (8.b)$$

where b'=K_{12}b, with b=*ag*I(z), H=([O_0]F'-1)/([O_0]F'), H'=N_2(1-0.67b't), with N_2=0.5(1+ k_8[A]/k_3)C_0F(N'P_0-0.5NbC_0F)/(F[O_0])^2; [O_0] is the initial oxygen concentration.
Eq.(8.b) shows that S_2 is a decreasing function of z and UV intensity, since b=*aq*I(z). We note that for the case of P_0=0, S_2 depends only on the UV light dose, ie., it has the same steady-stae for the same dose. However, for P_0>0, S_2 is higher for lower intensity (with the same dose) to be shown later.
Above S formulas show that NOM-type-I efficacy (S_1) is proportional to the initial RF concentration [A](C_0F)/(*aq*I_0), with no contribution from oxygen [O_2]; whereas S_2 is proportional to both [A]C_0(z,t) and the initial oxygen concentration, [O_0]. Therefore, resupply of RF solution, under a so-called controlled-concentration-method (CCM) during the UV exposure will increase significantly the overall efficacy, specially for accelerated CXL which has lower efficacy than the standard Dresden low-power (under non-controlled concentration) [13].

Similarly, for the second term of Eq. (5.a) for OM-type-I efficacy is given by, S_{12}=(s_1/s_2)S_2. Typical values are: f = 0.5 and s_1 = 0.01, and s_2 = 0.49 (for riboflavin). Knowing the S functions of type-I and type–II, the normalized overall CXL efficacy is given by Ceff=0.5[CX1 + CX2], with CX1=1-exp(-S_1), CX2=1-exp(-S_2), which is better than our previous formula [10] Ceff=1-exp[-(S_1+S_2)], because S_1 and S_2 have different basis in normalization, based on available monomers (in NOM-type-I) and substrate (in OM-type-II), in addition to deferent rate constants.

3.3 Dynamic profiles

Fig. 4 shows the numerical results of Eq. (3) for oxygen and RF concentration profiles for intensity I_0= (3,9,18) mw/cm^2 and z=0; using a fit N=10, for depletion time t_0 = (20,7) s for I_0= (3,9) mW/cm^2, for C_0=0.1, f=q=0.5, a=0.62. The fit-N is used to achieve oxygen profiles matching the similar trends of the measured data of Kamaev [2]. Other input parameters are used [2,4]: $[O_0]$=7.3, k_5/k_3=1, k_8/k_3=0.05, [A]=1.0, K'= $(s_1+s_2)/(1+C+0.65\,[A])$, $k_{72}=k_{71}=1.7\times10^5$ (1/s), $k_6=k_{11}=k_{12}=2.6\times10^5$ (1/s), D=500 um, D'=200 um, s_1=0.01, s_2=0.49, and P_0=0.05.

Fig. 4 shows that RF concentration, C(z,t), has a much slower decaying rate (about 5 times) than oxygen profiles. This can be easily realized by the RF effective rate $K_{12}(C_0F)^2b$ which is much smaller than the decaying rate of oxygen, $NbK_{12}C_0F$, (with N=10).

Fig. 5 shows the type-II efficacy (S_2) for intensity I_0= (3,9,18) mW/cm^2. If no oxygen supply (for P_0=0), all intensities have the same steady state value. However for P_0>0, higher intensity has a faster rising curve, but a lower steady state value due to the oxygen profiles in Fig. 4. In comparison, Fig. 6 shows the S-function profiles for NOM-type-I(S_1), the first term of Eq. (5.a), for intensity I_0= (3,9,18,30) mW/cm^2, based on analytic formula, Eq. (8.a) [9,11].

Eq. (8) and (9) show that NOM-type-I efficacy (S) is proportional to $[A](C_0F)/(aqI_0)$, but not oxygen $[O_2]$, whereas OM-type-II efficacy (S_2) depends on both C(z,t) and $[O_2]$. Moreover, both S_1 and S_2 have similar trend that lower steady state efficacy in higher intensity. However, they have opposite trends on their z-dependence, where NOM-type-I (type-II) is an increasing (decreasing) function of z [9-11], for the anterior range of z<400 um.

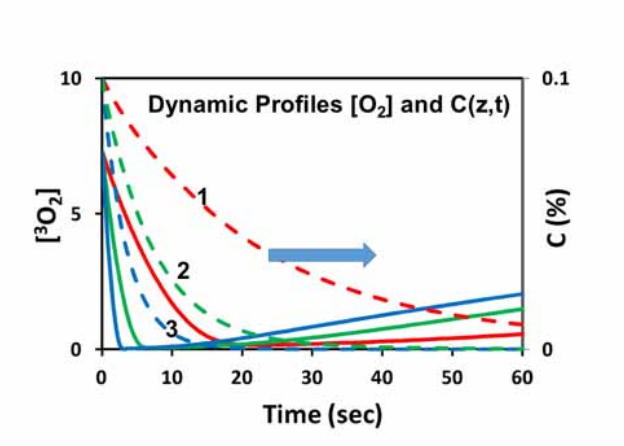

Fig. 4 The dynamic profiles of gorund state oxygen (solid curevs) and riboflavin (dashed curves) concentration (on surface, z=0), for intensity I_0= (3,9,18) mW/cm^2

(for curves in red, green, blue), for C_0=0.1%, [O_0]=7.3 mg/L and oxygen supply rate P_0=0.05 (1/s).

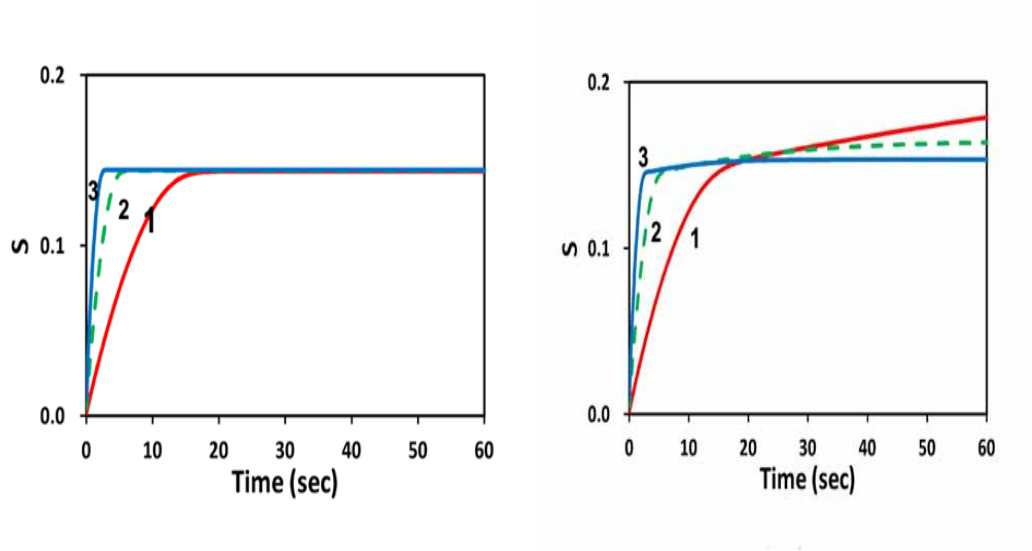

Fig. 5 The S-function profiles for Type-II (S_2) associate to Fig. 4, but for P_0=0 (left figure) and P_0=0.05 (right figure)..

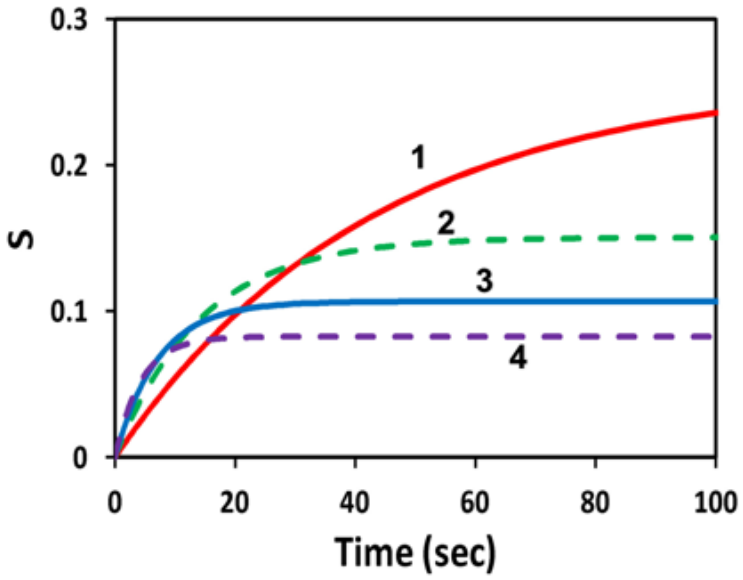

Fig. 6 The S-function profiles for Type-I(S_1) (at z=0), for intensity I_0= (3,9,18,30) mW/cm^2 (curves 1,2,3,4), for C_0=0.1% and D=500 um, based on analytic formula Eq. (8.a).

3.4 Summary of important CXL features

From the analytic formulas Eq. (5) to Eq. (8) and the calculated data shown in Figs. 4 to 6, the key features of type-I and type-II CXL are summarized and compared as follows:

(a) Oxygen is required for ROS-mediated type-I and type-II CXL, but it is not required in NOM-mediated type-I. The ratio in RF depletion and efficacy due to OM and NOM-type-I is defined by R=3/[A]. Therefore, for large substrate concentration (with [A]>10 mg/L), type-I is dominant; whereas when [A]<1 mg/L, type-II-OM is dominant but only plays a limited and transient state role for $t<t_0$, with t_0 being the depletion time of oxygen.

(b) As shown by Fig. 4, in the transient stage (about 3 to 20 seconds), both type-I and type–II coexist until the oxygen is depleted; then type-I dominates before the oxygen is resupplied or replenished. Fig. 4 also shows that RF depletion is much slower than that of oxygen (Fig. 4). Therefore, at the time oxygen is depleted, (or OM-type-II reaches its steady-state efficacy), about 40% of RF is still available to achieve NOM-type-I process.

(c) Both type-I and type-II efficacy are nonlinear increasing function of the UV light dose (or fluence) in the transient state. but they have different functional forms given by Eq. (5). Type-II and OM-type-I efficacy have similar functional form and are proportional to bt, or the UV light dose (I_0t); whereas the NOM-type-I is proportional to $I_0^{-0.5}$, or $t^{0.5}$, for a given dose [9,11].

(d) Both NOM-type-I and type-II shows the similar trend that higher intensity has lower steady-state efficacy, as shown by Fig. 5 and 6.

(e) NOM-type-I has a steady-state efficacy increasing to the depth (z), whereas type-II and OM-type-I has opposite trend, decreasing function of z.

(f) Larger diffusion depths (D or D') achieve higher efficacy in both type-I and II, as shown by the diffusion equations, F=1-0.5z/D and F'=1-0.5z/D'.

(g) In OM process, higher intensity depletes oxygen faster and its efficacy reaches a lower steady state. Same dose achieves same steady state OM efficacy (independent to the intensity) with the absence of oxygen replenishment, or when the source term P=0. However, lower intensity has higher steady state OM efficacy when P>0, as shown by Fig.5.

(h) RF depletion in type-I is partially compensated by the RF regeneration in the presence of oxygen given by the g factor in Eq. (3.a) which is a decreasing function of oxygen.

(i) The overall CXL efficacy, given by CX1+ CXL2, is governed by the time integration of I(z)C(z,t) and $I(z)[O_2]C(z,t)$, for type-I and type–II, respectively. When either C(z,t) or $[O_2]$ is largely depleted, the CXL efficacy reaches its saturation level which can not be improved by applying a higher dose (or longer

exposure time), unless there are resupply of C(z,t) and/or [O_2] during the UV exposure. A so-called RF concentration-controlled method (CCM) was proposed for type-I [13]. Similarly, one may improve the type-II efficacy by external supply of high-pressure-oxygen, rather than its natural diffusion from air.

This study focuses on the derivation of analytic formulas and predicted features derived from them, whereas greater details of the roles of each of the components on the overall CXL efficacy will be shown elsewhere by numerical solution of Eq. (5), including diffusion depth (D, D'), quantum yield (q), RF depletion rate (*aqg*I), oxygen depletion rate (Nb), and the oxygen source term (P_0). The formulas developed in this study provide guidance for further clinical studies. The features predicted in this study are based on a modeling system which may not represent a real CXL system. Moreover, parameters (or the rate constants k_j) used in the calculatuons would require further clinical measurement for more accurate values. Greter details on the debating issues and a critical review on the kinetic and efficacy and optimal protocols of CXL will be published elsewhere.

4. CONCLUSION

In the transient state (5 to 20 seconds), CXL efficacy is governed by both type-I and –II mechanisms, and after that period the NOM-type-I is dominant, while oxygen for OM-process only plays a transient role, in contrary to the conventionally believed OM-dominant mechanism. A new protocol using CCM can improve the efficacy in accelerated CX, which is less efficient than the Dresden (low intensity) CXL under the normal, non-controlled methods.

CONSENT

It is not applicable.

ETHICAL APPROVAL

It is not applicable.

COMPETING INTERESTS

The author is the CEO of New Vision Inc. and has financial interest.

REFERENCES

1. Hafezi F and Randleman JB. editors. Corneal Collagen Cross-linking, second ed.

Thorofare (NJ): SLACK; 2017.
2. Kamaev P, Friedman MD, Sherr E, Muller D. Cornea photochemical kinetics of corneal cross-linking with riboflavin. Vis. Sci. 2012;53:2360-2367.
3. Schumacher S, Mrochen M, Wernli J, Bueeler M, Seiler T. Optimization model for UV-riboflavin corneal cross-linking. Invest Opthamol Vis Sci. 2012; 53:762-769.
4. Semchishen A, Mrochen A, Semchishen V. Model for optimization of the UV-A/Riboflavin strengthening (cross-linking) of the cornea: percolation threshold. Photochemistry and photobiology, 2015; 91:1403-1411.
5. Kling S, Hafezi F. An algorithm to predict the biomechanical stiffening effect in corneal cross-linking. J Refract Surg 2017; 32:128-136. doi:10.3928/1081597X-20161206-01.
6. Caruso C, Epstein RL, Ostaacolo C, et al. Customized cross-linking- A mathematical model. Cornea, 2017; 36:600-604.
7. Lin JT, Liu HW, Cheng DC. On the dynamic of UV-light initiated corneal cross linking. J. Med Biolog Eng. 2014; 34: 247-250. doi: 10.5405/jmbe.15332.
8. Lin JT. Analytic formulas on factors determining the safety and efficacy in UV-light sensitized corneal cross-linking. Invest Ophthalmol Vis Sci 2015; 56:5740-574.
9. Lin JT. Combined analysis of safety and optimal efficacy in UV-light-activated corneal collagen crosslinking. Ophthalmology Research. 2016; 6(2):1-14. DOI{10.9734/OR/2016/28712.
10. Lin JT. Photochemical Kinetic modeling for oxygen-enhanced UV-light-activated corneal collagen crosslinking. Ophthalmology Research, 2017;7:1-8. DOI: 10.9734/or/2017/35032.
11. Lin JT, Cheng DC. Modeling the efficacy profiles of UV-light activated corneal collagen crosslinking. PloS One. 2017;12:e0175002. DOI:10.1371/journal.pone.0175002.
12. Lin JT. Efficacy and Z* formula for minimum corneal thickness in UV-light crosslinking. Cornea, 2017: 36:30-31. DOI:10.1097/ico.0000000000001269.
13. Lin JT. A Critical Review on the Kinetics, Efficacy, Safety, Nonlinear Law and Optimal Protocols of Corneal Cross-linking. J Ophalmology & Visual Neuroscinece, 2018; 3:017.
14. Lin JT. A proposed concentration-controlled new protocol for optimal corneal crosslinking efficacy in the anterior stroma Invest. Ophthalmol Vis Sci. 2018 (in press).
15. Wernli J, Schumacher S, Spoerl E et al. The efficacy of corneal cross-linking shows a sudden decrease with very high intensity UV light and short treatment time. Invest Ophthalmol Vis Sci. 2013;54:1176–80. [PubMed].

16. Zhu TC, Finlay JC, Zhou X, et al. Macroscopic Modeling of the singlet oxygen production during PDT. Proc SPIE. 2007; 6427:6427O81–6427O812.
17. Kim MM, Ghogare AA, Greer A, Zhu TC et al. On the in vivo photochemical rate parameters for PDT reactive oxygen species modeling. Phys. Med. Biol. 62 (2017) R1–R48.